Article:
Eom, H.H., Kim, H., Harbottle, D. et al. (2024) Selective removal of Cs+ and Sr2+ by electrosorption using intercalating titanosilicate. Separation and Purification Technology, 330 (Part C). 125550. ISSN: 1383-5866

https://doi.org/10.1016/j.seppur.2023.125550

Selective removal of Cs^+ and Sr^{2+} by electrosorption using intercalating titanosilicate

Ho Hyeon Eom[a], Hyunjung Kim[a], David Harbottle[b], and Jae W. Lee[a]*

[a] Department of Chemical and Biomolecular Engineering, Korea Advanced Institute of Science and Technology (KAIST), Daejeon 34141, Republic of Korea

[b] School of Chemical and Process Engineering, University of Leeds, Leeds LS2 9JT, United Kingdom

*Corresponding author
E-mail addresses: jaewlee@kaist.ac.kr (J. W. Lee)

Abstract

The utilization of ion intercalate capacitive deionization technology is garnering attention as an electrified water treatment method. This study proposes a capacitive deionization technology incorporating Dual-cation TitanoSilicate (DTS) to enable efficient electro-sorption/desorption of radioactive ions Cs and Sr. The synthesized DTS possesses a robust structure, high selectivity for Cs and Sr, and substantial adsorption capacity, incorporating redox-active titanium. Employing DTS as an active material in the electrode demonstrated a high adsorption capacity (186 mg Cs/g, 177 mg Sr/g) and rapid adsorption kinetics, reaching maximum capacity within 30 minutes, even in environments with a tenfold excess of competing ions. Furthermore, our system exhibited stable performance over 5 cycles of adsorption/desorption, and post-desorption analyses confirmed the durable structure stability without significant alterations. This study highlights the feasibility of CDI technology utilizing DTS for cesium and strontium removal.

Keywords

Capacitive deionization; Remediation; Electro-regeneration; Radionuclide; Titanosilicate

1. Introduction

The electricity demand has been steadily increasing worldwide for several decades [1,2]. The CO_2 emissions generated to meet this electricity demand have led to global climate change, causing abnormal climate phenomena around the world[3,4]. Various countries and industries are making efforts to curb carbon emissions. Prominently, energy-efficient processes are being designed to mitigate carbon generation[5–7], and strategies include capturing emitted carbon dioxide[8–10] and utilizing it to produce valuable materials[11,12]. Moreover, a transition towards renewable energy sources in electricity generation is underway. However, there are evident limitations in swiftly meeting the escalating electricity demand with environmentally friendly generation technologies[13]. To minimize carbon emissions while meeting the growing electricity demand, many countries have turned to nuclear power generation. However, behind the advantage of almost zero carbon emissions, there are drawbacks, including the generation of radioactive waste without immediate disposal solutions and the risk of radioactive material leakage. In particular, the radioactive isotopes Cesium-137 and Strontium-90, which are prominent among the radioactive elements generated in nuclear power plants, emit strong radiation, and have a very long half-life of 30 years[14,15]. In the event of accidents like Fukushima, these hazardous substances can be released into the natural environment through various pathways such as water and air, penetrating into the biological population. Furthermore, Cs and Sr behave similarly to the essential elements K and Ca in living organisms, leading to their accumulation in organs and bones, causing health issues and subsequent biological accumulation through the food chain[16,17]. Therefore, the development of technologies for the rapid and efficient treatment of these radioactive isotopes is urgently needed.

Various approaches, such as adsorption[18], ion exchange[19,20], coagulation[21,22], precipitation[23,24], and membrane separation[25–27], have been proposed to remove Cs and Sr, which are highly soluble in water. Among these, adsorption methods have been extensively studied due to their advantages of easy operation and low energy consumption. Different materials, including inorganic materials[18,19], Metal Organic Frameworks (MOFs)[28], carbon materials[29], and polymers[30], have been investigated for their potential in adsorption. However, simple adsorption methods have been criticized for their low adsorption capacity and low regeneration efficiency. Moreover, for non-inorganic materials, stability issues may arise due to radiation exposure[31].

Ion exchange, a water treatment method similar to adsorption, offers the advantage of selectively adsorbing ions using ion exchange materials, leading to high adsorption capacity. Representative inorganic ion exchange materials include metal hexacyanoferrates (MHCFs)[28,32], metal chalcogenides[19], and titanosilicates[18,33–37]. However, ion exchange processes still have drawbacks, such as the use of high concentrations of acid or alkaline solutions for regeneration, or the use of toxic extracting agents, which may lead to secondary contamination[38]. To achieve higher adsorption capacity and faster adsorption kinetics, it is efficient to reduce the size of the adsorbent particles to increase the surface area. However, using small adsorbent particles alone in water treatment processes can lead to drawbacks such as pressure drop. Therefore, they are often used in combination with various supports to address these challenges[39].

Electrochemical adsorption has also garnered significant attention as a desalination method in recent years[40–42]. The fundamental concept of capacitive deionization (CDI) relies on utilizing the potential difference between electrodes to create an electrical double layer, where ions with opposite charges are adsorbed and removed. CDI is characterized by low voltage and low energy consumption, and one of its major advantages is the ability to desorb ions by applying a reverse voltage during the regeneration process. One of the drawbacks of the conventional CDI technology is the difficulty in imparting ion selectivity[43,44]. Since all charged ions form electrical double layers and are removed, it becomes challenging to efficiently utilize the adsorption capacity of the electrode when specific ions need to be removed from high salinity solutions, such as groundwater or seawater. However, by utilizing ion intercalation materials, not only can selectivity be enhanced, but also higher capacities can be anticipated[45].

Therefore, our aim is to design electrodes for CDI processes that incorporate ion exchange materials as the active material, providing high ion selectivity, rapid adsorption, and easy regeneration. As mentioned earlier, although there are various candidates for ion exchange materials, to apply them to CDI for Cs and Sr removal, they need to selectively adsorb each ion and be electrochemically stable. Titanosilicate-based ion exchange materials meet these criteria. Among the types of titanosilicates, ETS-4[33], ETS-10[34], CST[35], AM-4[36,37], and DTS[18]are representative. Among them, DTS exhibits high adsorption capacity for both Cs and Sr and also demonstrates high ion selectivity[18], making it highly suitable for application in CDI technology. We fabricated an intercalative electrode utilizing DTS as an ion-selective adsorption site, enabling the adsorption of target ions even in environments with competing ions.

This study proposed the utilization of DTS to fabricate electrodes for CDI and investigated their physicochemical and electrochemical properties through various analyses. Furthermore, we assessed the applicability of DTS electrodes in the treatment of radioactive wastewater by selectively or simultaneously removing Cs and Sr. By analyzing the results of electrochemical adsorption and desorption experiments using DTS electrodes, we identified the optimal CDI operation conditions and verified the potential of DTS for multicycle operations.

2. Material and Methods

2.1. Materials

1-methyl-2-pyrrolidinone (NMP, 99.5 %), polyvinylidene fluoride (PVDF, average MW ~534,000), potassium fluoride (99%), sodium silicate ($Na_2O(SiO_2)_x \cdot xH_2O$), strontium chloride hexahydrate ($SrCl_2 \bullet 6H_2O$, 99%), titanium (III) chloride ($TiCl_3$, 12 wt.% TiCl3 in hydrochloric acid) were purchased from Sigma-Aldrich. Potassium chloride (KCl, 99%), sodium chloride (NaCl, 99.5%), and sodium hydroxide (NaOH, 97%) were supplied by JUNSEI Chemical. Carbon black (Super P) and cesium chloride (CsCl, 99.999%) were purchased from Alfa Aesar. Potassium hydroxide (KOH, 95%) was obtained from SAMCHUN CHEMICALS. All chemicals were used as received without further purification and all aqueous solutions were prepared using Milli-Q water (Millipore).

2.2. Synthesis of Dual-cation (Na^+ and K^+) incorporated TitanoSilicate (DTS)

The Ivanyukite-type titanosilicate incorporating Na and K was synthesized as previously reported through a hydrothermal reaction[18]. In detail, the following steps were carried out under ambient temperature and pressure conditions prior to the hydrothermal reaction. First, titanium chloride (12.8 g) was mixed with deionized water (54 g). Sodium silicate (11 g) was added to the titanium chloride solution with vigorous stirring. Then, a mixture of sodium hydroxide (9 g), potassium hydroxide (4.5 g), and potassium fluoride (4.7 g) was added to the vigorously stirred solution. The final mixture was thoroughly mixed until the color changed from dark blue to milky-white. Subsequently, the mixture was transferred to a 100 mL teflon-lined autoclave, sealed, and placed in a preheated oven at 180℃ for a 4-day reaction period. After the reaction, the resulting product was washed alternately with DI water and ethanol and then dried at an oven to obtain DTS.

2.3. Fabrication of DTS electrode

The synthesized DTS powder (2 g), conductive agent Super P (0.25 g), and binder polyvinylpyrrolidone (PVDF, 0.25 g) are mixed to manufacture a homogeneous slurry through ball-milling. The ball-milling conditions are as follows: DTS, carbon black, PVDF, and 20 mL of NMP are placed in a 50 mL zirconium oxide jar, and zirconium oxide balls with a diameter of 1 mm are added to fill the jar. The zirconium oxide jar is securely sealed, and the mixture is milled at a speed of 400 rpm for 6 hours to produce a uniform slurry.

The slurry is then drop-coated onto a stainless-steel mesh (500 mesh) prepared in a size of 1×2 cm^2. The drop-coating is done in a 1×1 cm^2 area. The amount of slurry is adjusted to achieve a loading mass of 1 mg after drying in a 70°C vacuum oven for 24 hours, ensuring complete removal of NMP.

2.4. Detailed Electrochemical Experimental Methodology

All electrochemical experiments were conducted using a stainless-steel mesh with the DTS slurry as the working electrode, a platinum coil as the counter electrode, and Ag/AgCl (3.0 M KCl) as the reference electrode in a three-electrode system. The electrochemical experiments were controlled and analyzed using a Biologic potentiostat. As a basic electrolyte, a 20 mM NaCl solution (10 mL) was used during the activation and deintercalation stages, while during the electro-sorption stage, a solution consisting of 20 mM NaCl and 1 mM CsCl or $SrCl_2$ (10 mL) was used.

The activation stage was performed as a priority before using each working electrode, and no additional activation was conducted during the experiments. Activation consisted of two steps, which included cyclic voltammetry and deintercalation. Cyclic voltammetry was conducted with a potential window of -1.0 V (vs. Ag/AgCl) to 0.5 V at a scan rate of 50 mV/s for 5 cycles. During the deintercalation step, a voltage of +2.0 V (vs. Ag/AgCl) was applied for 0.5 hours to remove pre-existing Na and K ions.

In the electro-sorption/desorption stage, the electrolyte was stirred at 200 rpm while applying specific voltages (electro-sorption: Open Circuit Voltage to -1.2 V, electro-desorption: +2.0 V) for predefined durations, and the concentration of the solution was measured and utilized. However, when measuring the distribution coefficient according to the Na ratio, the electrolyte was prepared by adding NaCl to a concentration of 1 ppm Cs or Sr as a reference.

$$Adsorption\ amount\ (mg/g) = \frac{V}{m}(C_0 - C_{ads,t}) \quad (1)$$

$$Distribution\ coefficient\ (K_d, mL/g) = \frac{V}{m}\frac{(C_0 - C_{ads,t})}{C_{ads,t}} \quad (2)$$

$$Desorption\ amount\ (mg/g) = \frac{V}{m}(C_{des,t}) \quad (3)$$

$$Regeneration\ percent\ (\%) = \frac{C_{des,t}}{C_0 - C_{ads,t}} \times 100 \quad (4)$$

In the equations, C_0 and C_t represent the electrolyte concentration at the initial and arbitrary time points, respectively. V and m denote the effluent volume and the mass of the composite composed of DTS, Super P, and PVDF, respectively.

2.5. Characterization

The X-ray diffraction pattern was analyzed using an Ultima IV instrument (Rigaku) with Cu Kα1 as the X-ray source to obtain structural information. Morphological information and the elemental composition were acquired using a scanning electron microscope (SEM; SU5000, Hitachi) coupled with energy-dispersive spectroscopy (EDS).

For the analysis of elemental species and their chemical states, X-ray photoelectron spectroscopy (XPS; K-alpha, Thermo) was utilized with a micro-focused monochromatic Al Kα source (1486.7 eV). The C 1s peak was referenced to 284.8 eV using Thermo Avantage software for accurate measurements.

The concentration of the electrolyte was determined using inductively coupled plasma-optical emission spectroscopy (ICP-OES 5110, Agilent) and inductively coupled plasma-mass spectroscopy (ICP-MS, Agilent). These analytical techniques provided valuable information on the elemental composition, chemical states, and electrolyte concentration, enabling a comprehensive characterization of the studied material.

3. Results

3.1. DTS electrode characterization

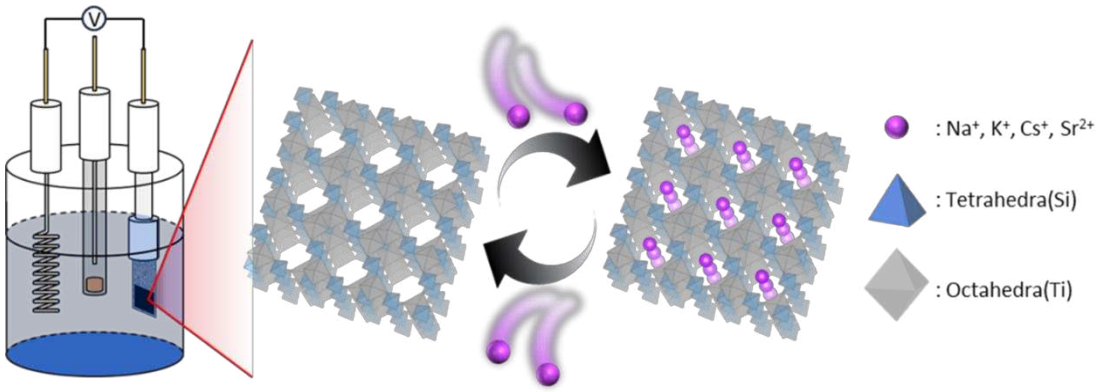

Fig. 2 Schematic illustration of electro-sorption and regeneration using DTS Electrode for Cs^{+} and Sr^{2+} removal.

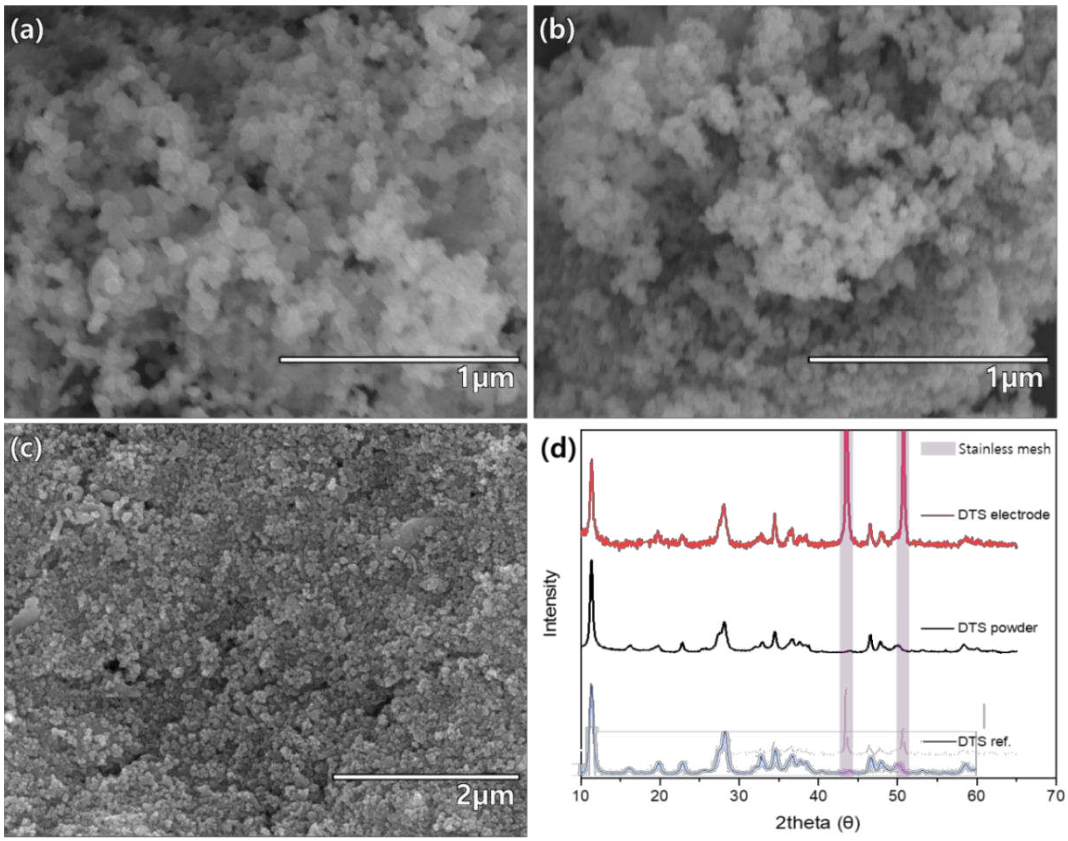

Fig. 1 SEM images of (a) DTS powder, (b) Super P, and (c) as-prepared DTS electrode. (d) XRD patterns of as-prepared DTS electrode (red), DTS powder (black), and DTS powder from a previous work (blue)[18].

Dual-cation Titano-Silicate (DTS) was synthesized using the same method as in the previous study[18] and its morphology was observed through SEM images, revealing the presence of cubic-shaped particles with sizes in the range of tens of nanometers, agglomerated together

(Fig. 2a). XRD analyses of the sample showed characteristic peaks at 11.4°, 28.2°, as well as 16.2°, 19.7°, and 22.9°, confirming the successful formation of pharmacosiderite-type titanosilicate, consistent with previous reports (Fig. 2d). Additionally, SEM-EDS images confirmed the coexistence of Na and K, indicating the successful preparation of DTS (Fig. S1).

The synthesized DTS was dispersed in the NMP solvent along with Super P and PVDF using a ball mill to create a slurry, and drop coating was employed to fabricate the DTS electrode on a stainless-steel mesh. SEM images also revealed the uniformity of the electrode fabrication (Fig. 2c). The XRD analysis of the freshly prepared DTS electrode revealed no structural changes during the slurry preparation process using a ball mill, and distinctive peaks of the stainless-steel mesh, which functioned as the current collector, emerged at 43.6° and 50.7° (Fig. 2d).

In this study, the robust framework of DTS, composed of SiO_4 tetrahedra and TiO_6 octahedra, facilitated the adsorption and desorption of various cations into the tunnels under different voltages. By leveraging the ion selectivity of DTS, Cs^+ and Sr^{2+} were effectively separated during the process, as illustrated in Figure 1.

3.2. CV curves and electro-sorption of Cs^+ and Sr^{2+}

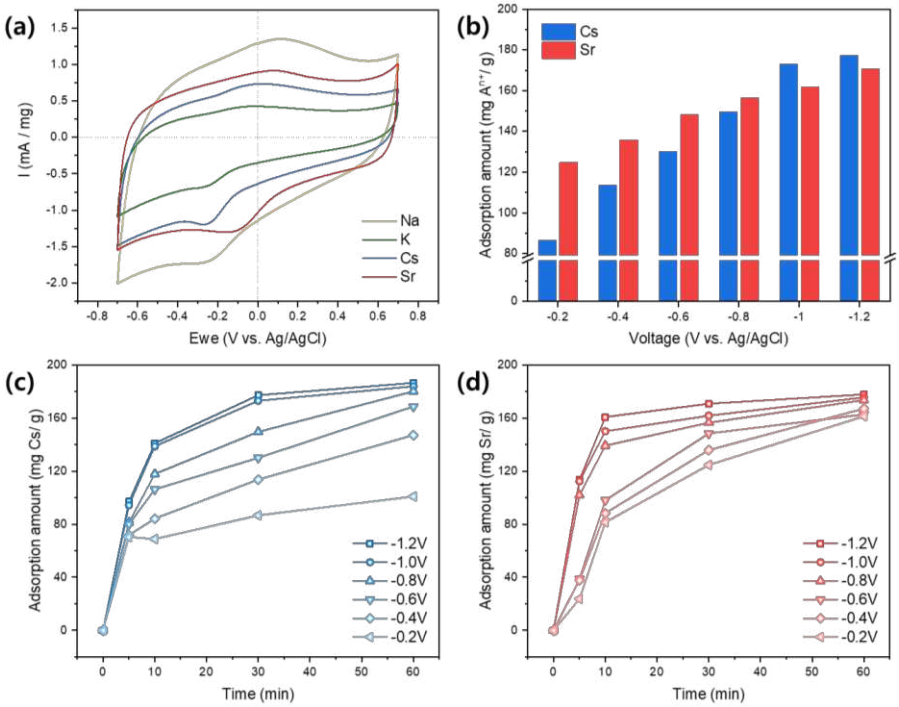

Fig. 3 (a) Cyclic voltammogram of DTS electrode in various solutions (50mM NaCl, KCl, CsCl, or $SrCl_2$) at 100 mV s^{-1}; (b) electrosorption quantities of DTS electrode in 20mM NaCl + 1mM CsCl or $SrCl_2$ at different working electrode voltages for 0.5 h. Electro-sorption kinetics of DTS electrode at different working electrode voltages in (c) 20mM NaCl + 1mM CsCl, and (d) 20mM NaCl + 1mM $SrCl_2$.

To comprehend the electrochemical characteristics of the fabricated DTS electrode, cyclic voltammetry (CV) was conducted (Fig. 3a). Prior to the CV measurement, the DTS electrode was subjected to a potential of +2.0 V (vs. Ag/AgCl) to remove the intercalated Na and K ions from the 8-membered ring tunnel, composed of Ti_4O_{16} clusters and SiO_4 tetrahedra, to

investigate the electrochemical interactions of DTS with single cations (Fig. S2). Subsequently, CV experiments were performed using a 50mM metal chloride solutions, with a potential window ranging from -0.7 V to 0.7 V and a scan rate of 100 mV/s. Due to the smaller size of Na ions, they exhibited a higher specific capacitance compared to that in the KCl solution[46]. Cs and Sr ions, which have sizes similar to that of K ions, showed even higher peak currents and specific capacitance than those observed under KCl solution conditions, owing to their strong reactivity with DTS.

For the monovalent cations solutions, a cathodic peak appeared around -0.3 V to -0.2 V was observed, whereas in strontium chloride solution, the cathodic peak emerged around -0.1 V. The corresponding anodic peak was observed within the range of -0.05 V to 0.1 V. This peak pair is attributed to the redox couple involving Ti(IV) and Ti(III)[47].

Table 1. Comparison of Cs^+ and Sr^{2+} adsorption capacity for various adsorbents.

	Method	$Q_{m,Cs}$ (mg/g)	$Q_{m,Sr}$ (mg/g)	Voltage (V)	Reaction time (hour)	$C_{0,Cs}$ (ppm)	$C_{0,Sr}$ (ppm)	Reference
Prussian blue nanorod	Batch adsorption	205	265	-	3	500	500	[48]
Na26L & K26L	Batch adsorption	415	105	-	8	12000	1500	[49]
ETS-1	Batch adsorption	332	133	-	3	1500	1500	[33]
ETS-2	Batch adsorption	295	159	-	3	1500	1500	[33]
ETS-4	Batch adsorption	238	39	-	3	1500	1500	[33]
DTS	Batch adsorption	469	179	-	-	1500	750	[18]
DTS	electro adsorption	186	177	-1.2	1	133(Cs) +460(Na)	88(Sr) +460(Na)	This work
Activated carbon cloth	electro adsorption	18	22	-1.2	2	20	20	[50]

(Tianxiang Co., Ltd)								
CuHCF	electro adsorption	218	77	-1.4	1	100	100	[51]

Figure 3b illustrates the adsorption capacity of the DTS electrode in a 20mM NaCl solution with the addition of either 1mM CsCl or 1mM $SrCl_2$, under different voltages for a duration of 0.5 hour. When compared with the results of adsorption experiments conducted within a voltage range (-0.2 V to -1.2 V) where water electrolysis does not occur to ensure sustainable operation, it was observed that the highest adsorption capacities for both Cs^+ and Sr^{2+} were achieved at the most negative voltage of -1.2 V[52].

Additionally, prior to evaluating the performance of the electro-sorption/desorption cycle using the DTS electrode, electro-sorption kinetics was determined (Fig. 3c, d) to determine the optimal adsorption time. As the applied voltage increased and the adsorption time prolonged, the adsorption capacity also increased. For Cs^+, the maximum adsorption capacity was observed to be 186 mg Cs^+/g, while for Sr^{2+}, it was approximately 177 mg Sr^{2+}/g. Notably, for Cs^+, the measured adsorption capacity was lower than the known Cs^+ adsorption capacity of DTS. This aspect will be further addressed in the subsequent sections of this paper. Despite this, the use of DTS in electro-sorption processes exhibited remarkable adsorption capacities even at low concentrations, coupled with rapid adsorption rates (Table 1).

To comprehend the underlying factors contributing to the remarkable electro-sorption

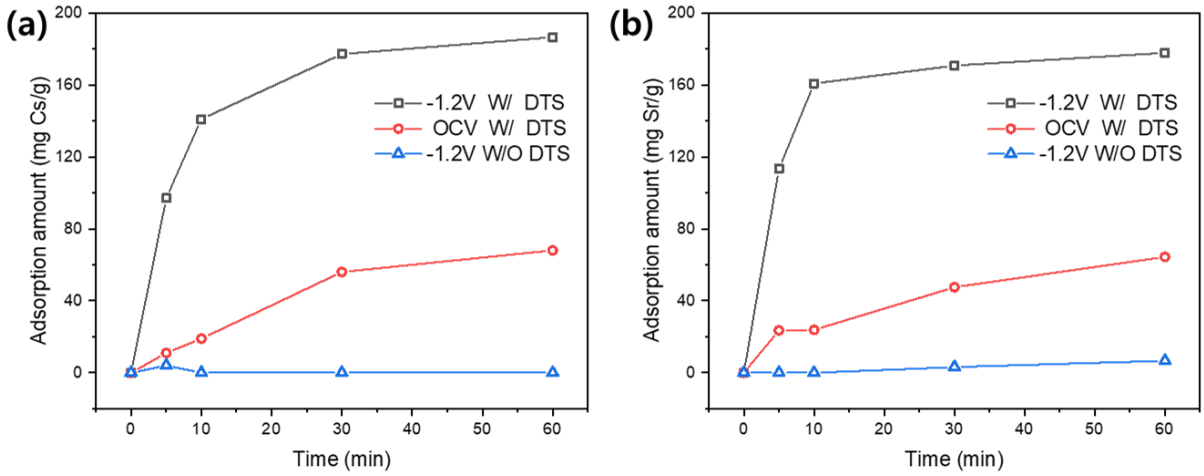

Fig. 4 Electro-sorption kinetics of (a) Cs^+ and (b) Sr^{2+} under different operating conditions and different DTS:Super P:PVDF ratios at -1.2V with 8:1:1 ratio(black), at 0 V with 8:1:1 ratio(red), and at -1.2V with 0:1:1 ratio(blue).

performance of the DTS electrode, two control groups were established, and electro-sorption kinetics were further analyzed, as illustrated in Figure 4. As a control group to investigate the electrochemical effects, DTS electrodes with the same composition of DTS, carbon material, and PVDF were used without applying any additional voltage during the adsorption process, indicated by the red line in the Fig. 4. Similarly, to demonstrate the effect of DTS, an identical

voltage of -1.2 V was applied, but this time, the electrode was composed only of carbon material and PVDF without DTS. The electro-sorption process was then carried out, and the results are represented by the blue line in Fig. 4. Through this, two facts were deduced. Firstly, the electrode composed of carbon and binder without DTS exhibited minimal adsorption efficiency compared to the electrode containing DTS. Secondly, although the known theoretical adsorption capacity of DTS is remarkably high, without electrochemical assistance, it is challenging to adsorb Cs^{+} and Sr^{2+} within a short period. However, when an external voltage is applied, adsorption occurs rapidly, suggesting the potential utilization of DTS for the swift treatment of radioactive-contaminated water.

3.3. Selective electro-sorption of Cs and Sr

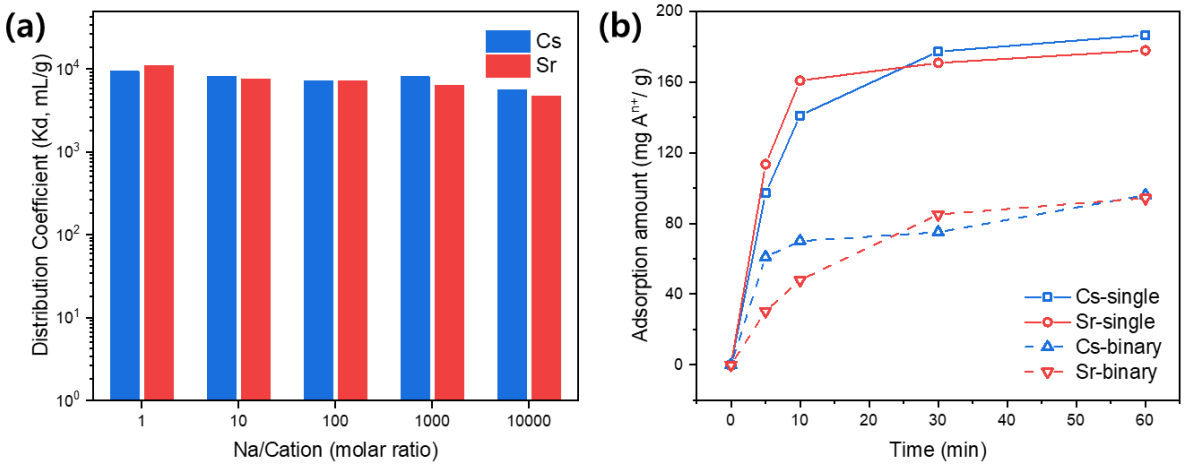

Fig. 5 (a) Distribution coefficients function of molar ration of Na/Cs and Na/Sr. (b) Electro-sorption kinetics of DTS electrode for Cs and Sr in binary solution (20mM NaCl + 1mM CsCl, + 1mM $SrCl_2$) at -1.2 V (vs. Ag/AgCl).

To be utilized as a material for treating radioactive-contaminated water, selectivity for the target species is considered a crucial factor. The results of evaluating the selectivity in the electro-sorption process of the DTS electrode are presented in Figure 5. In cases where actual removal of Cs and Sr from contaminated water is required, their concentrations are not typically high[53]. Therefore, Cs or Sr ions were fixed at a concentration of 1 ppm, and the distribution coefficient was measured and analyzed while increasing the molar ratio of Na (Figure 5a). Even in the presence of an aqueous solution with a 10,000-fold excess of Na ions, the electro-sorption process exhibited remarkably high selectivity, with a distribution coefficient of approximately 5000 mL/g for both Cs^{+} and Sr^{2+}, even during a short 0.5 hour adsorption process, demonstrating its potential as a highly selective process.

Furthermore, an analysis of the adsorption difference for each ion was performed during electro-sorption from a binary solution containing both ions, Cs and Sr (Figure 5b). The results of the electro-sorption kinetics analysis for the binary system showed a similar trend to that of the single-target ion solution, reaching maximum adsorption after 0.5 hours, with no significant difference in selectivity between the two ions. Therefore, it is believed that the inherent high selectivity of DTS for Cs and Sr ions is adequately utilized even in the electro-sorption process, which involves the rapid adsorption of a large quantity of ions in a short time.

3.4. Structural stability & regeneration tests

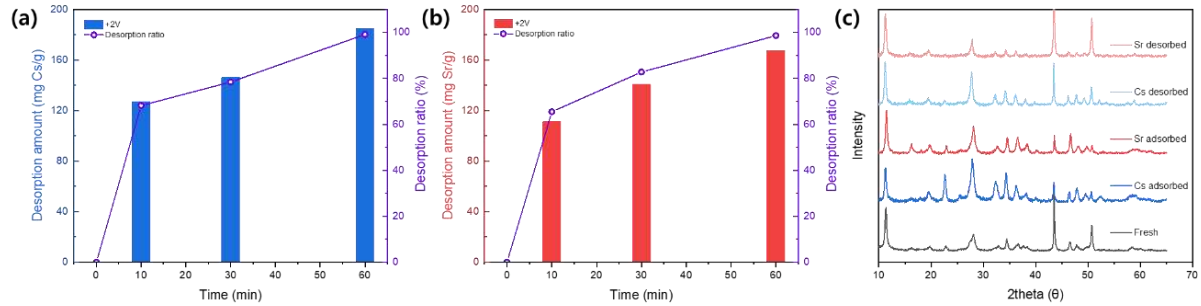

Fig. 6 Electro-desorption kinetics of DTS electrode for (a) Cs^{+} and (b) Sr^{2+} in 20mM NaCl electrolyte. (c) XRD patterns of as-prepared DTS electrode(black), Cs-adsorbed DTS electrode(blue), Sr-adsorbed DTS electrode(red), Cs-desorbed DTS electrode (light blue), and Sr-desorbed DTS electrode (light red).

In other water treatment processes that utilize adsorbents, the regeneration of the adsorbent is typically essential for economic viability. However, the regeneration process often involves the use of concentrated acids, alkaline solutions, or toxic substances, which may pose risks of environmental contamination and reduce sustainability. One significant advantage of the electrochemical water treatment method presented in this paper is the ease of regenerating the active material on the electrode by simply applying a reverse voltage. In Figure 6, electro-desorption kinetics was measured by applying a +2.0 V (vs. Ag/AgCl) voltage to the electrode with Cs or Sr adsorbed. After 0.5 hours of applying the reverse voltage, about 80% of the previously adsorbed ions were desorbed, and after one hour, over 98% regeneration was achieved. Remarkably, XRD analyses of the as-prepared DTS electrode, Cs or Sr adsorbed electrode, and Cs or Sr desorbed electrode showed that the structure composed of Ti octahedra and Si tetrahedra remained stable. Therefore, the electro-sorption/desorption process utilizing DTS as an active material, as proposed in this paper, can be considered an environmentally friendly process with cyclability and sustainability.

3.5. electro-sorption/desorption cycle performance

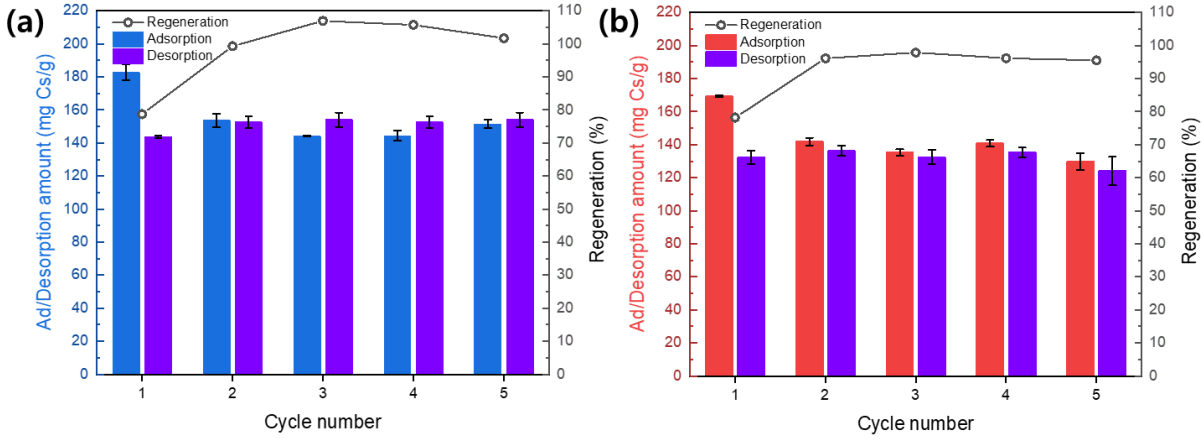

Fig. 7 Cycle tests of DTS electrode in (a) 20mM NaCl + 1mM CsCl, and (b) 20mM NaCl + 1mM $SrCl_2$. Electro-sorption at -1.2 V (vs. Ag/AgCl) for 0.5 h and electro-desorption at 2.0 V (vs. Ag/AgCl) for 0.5 h.

To assess the feasibility of applying the electro-sorption/desorption process repeatedly, a five-stage cycle test was conducted. Considering the rapid electro-sorption required for Cs and Sr ions, as indicated by the electro-sorption/desorption kinetics analysis, the adsorption conditions were set at -1.2 V (vs. Ag/AgCl) for 0.5 hours. For efficient desorption and minimal water electrolysis, the optimal operational conditions were established by performing a single cycle at +2.0 V for 0.5 hours.

In Figure 7, the results of the cycle test for Cs and Sr ions are illustrated. Stable electro-sorption/desorption cycles were observed from the second to the fifth cycle, except for the first cycle. Unfortunately, the first cycle exhibited the highest sorption capacity but resulted in incomplete desorption of adsorbed ions. This phenomenon can be attributed to the difficulty of completely deintercalating ions located deep within the DTS framework within a short desorption period of 0.5 hour, as evident from the electro-desorption kinetics. During the first cycle, only ions within a reachable distance from the electrode surface during the 0.5-hour desorption were effectively removed. From the second to the fifth cycle, stable performance of electro-sorption and desorption was observed, as ions closer to the electrode surface were consistently intercalated and deintercalated within the DTS framework. In the SEM image of the DTS electrode subjected to adsorption-desorption cycling, no discernible damage or alterations were observed (Fig S3).

3.6. Adsorption mechanisms

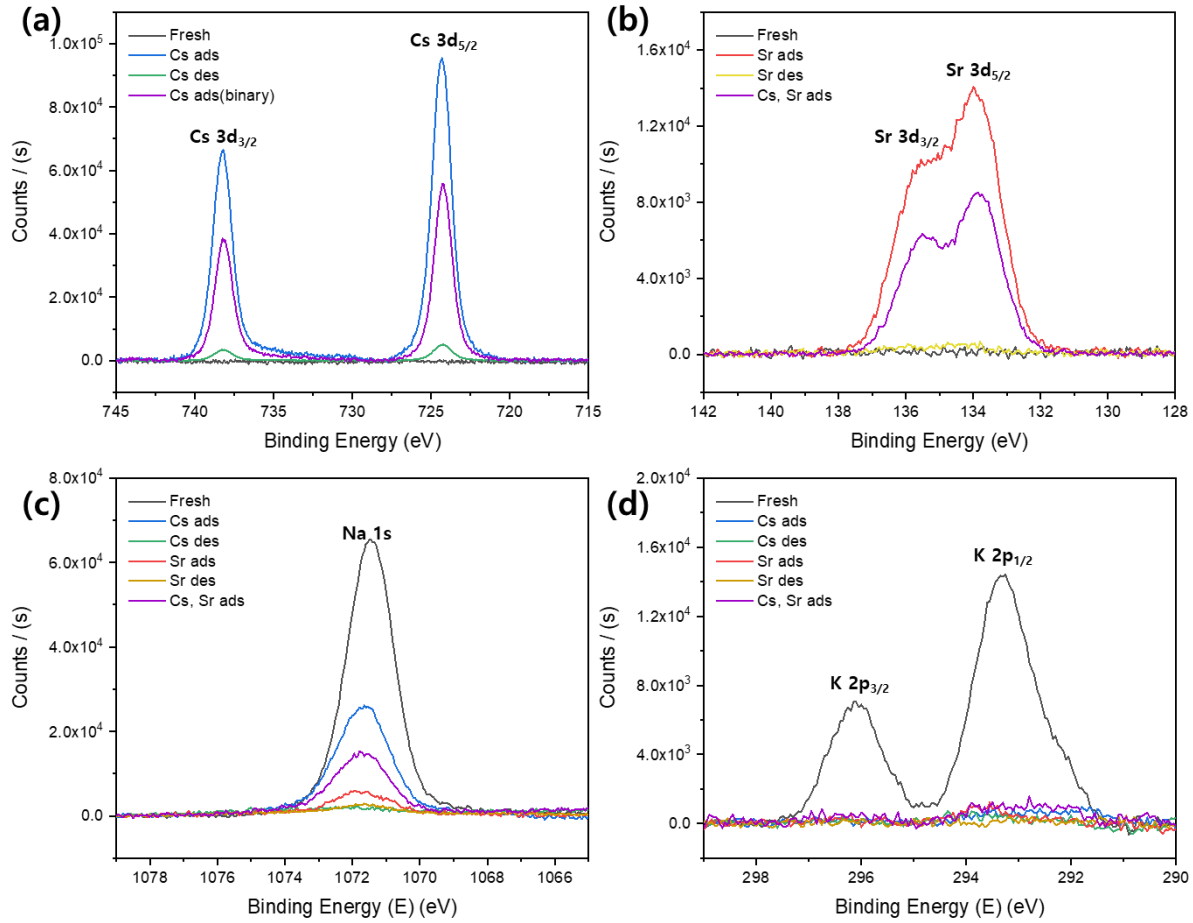

Fig. 8 XPS spectra of (a) Cs 3d, (b) Sr 3d, (c) Na 1s, and (d) K 2p for as-prepared DTS electrode, Cs adsorbed electrode, Cs desorbed electrode, Sr adsorbed electrode, Sr desorbed electrode, and Cs, Sr adsorbed electrode.

To analyze the ion adsorption mechanism of the DTS electrode, the XPS spectra of guest ions were presented in Fig. 7, from the initial stage of DTS electrode fabrication to each step of adsorption and deintercalation. The binding energies of each cation were determined as follows: Cs 3d at 738.2 and 724.3 eV, Sr 3d at 135.6 and 133.8 eV, Na 1s at 1071.7 eV, and K 2p at 293.2 and 296.1 eV (Fig. 8).

Regarding the behavior of Na and K ions, in the as-prepared fresh DTS electrode, distinct peaks of Na and K derived from DTS were observed. During the activation process, most of the Na and K ions were removed during the deintercalation stage of activation process. This behavior can be attributed to the characteristic ion exchange nature of DTS in the adsorption process. Contrarily, Na which exists in the electrolyte at a 20-fold molar ratio compared to the target ions, undergoes unavoidable adsorption due to electrostatic forces, as evidenced by the presence of the Na 1s peak. However, the quantity of Na 1s peak observed is lower compared to the as-prepared fresh electrode.

Notably, when adsorbing Sr, significantly fewer Na 1s peaks were observed compared to when adsorbing Cs. This observation is consistent with the adsorption capacity results. While DTS retained its intrinsic theoretical adsorption capacity during Sr electro-sorption, it did not maintain the same capacity during Cs electro-sorption. There is a study that has reported that the pharmacosiderite-type titanosilicate exhibits higher affinity for Sr than Cs[54]. This finding suggests that in the competition for adsorption with Na, the significantly higher affinity of Sr results in minimal Na adsorption, while Cs also exhibits higher selectivity against Na but lacks sufficient affinity to exclude Na present at a 20-fold concentration. This interpretation is further supported by the XPS spectra of Ti (Fig. S4). The binding energy of Ti 2p in the as-prepared DTS electrode was 458.6 eV, which increased to 458.74 and 458.94 eV upon Cs and Sr sorption. This suggests a stronger affinity in the order of $Sr^{2+} > Cs^{+} > Na^{+}$[55].

Examining the behavior of Cs and Sr ions during electro-desorption, it is confirmed that most of the Cs and Sr ions are removed, and simultaneously, the co-adsorbed Na is also efficiently removed, resulting in high regeneration efficiency.

4. Conclusions

We demonstrated the selective removal of Cs and Sr using the dual-cation titanosilicate (DTS) based capacitive deionization (CDI) technology, coupled with an environmentally friendly and straightforward electro-sorption/desorption regeneration method. Leveraging the distinctive feature of DTS, which provides a stable structure accommodating the intercalation of cations, we successfully removed cesium and strontium from water effluent. The system exhibited rapid adsorption kinetics with a maximum adsorption capacity within 1 hour, demonstrating a high adsorption capacity (186 mg Cs/g, 177 mg Sr/g). Furthermore, it allows for selective treatment in various sodium ratios of solutions, achieving maximum distribution coefficients (Cs: 9433 mL/g, Sr: 11123 mL/g). In contrast to the harsh regeneration methods employed in traditional adsorption-based water treatments, our approach enabled electrode regeneration with a simple application of a +2.0 V (vs. Ag/AgCl) overpotential. During the desorption process, no structural degradation was observed, and stable adsorption and desorption capacities were maintained over five cycles of adsorption-desorption. Our study provided the effective selective removal of radioactive Cs and Sr from waste aqueous solutions using the CDI method with DTS as an active electroadsorbent.

5. Acknowledgement

The authors are grateful for the financial support from the UK-Republic of Korea Joint Research Program (NRF-2022M2E9A2051171) through the NRF grants funded by the Ministry of Science and ICT, Republic of Korea. DH acknowledges the financial support of the Engineering and Physical Sciences Research Council (EPSRC, # EP/S032797/1).

Reference

[1] M.S. Bakay, Ü. Ağbulut, Electricity production based forecasting of greenhouse gas emissions in Turkey with deep learning, support vector machine and artificial neural network algorithms, J Clean Prod. 285 (2021). https://doi.org/10.1016/j.jclepro.2020.125324.

[2] A. Kasturi, G. Gug Jang, D. Stamberga, R. Custelcean, S. Yiacoumi, C. Tsouris, Determination of the regeneration energy of direct air capture solvents/sorbents using calorimetric methods, Sep Purif Technol. 310 (2023). https://doi.org/10.1016/j.seppur.2023.123154.

[3] P. Nejat, F. Jomehzadeh, M.M. Taheri, M. Gohari, M.Z. Muhd, A global review of energy consumption, CO2 emissions and policy in the residential sector (with an overview of the top ten CO2 emitting countries), Renewable and Sustainable Energy Reviews. 43 (2015) 843–862. https://doi.org/10.1016/j.rser.2014.11.066.

[4] T. Gasser, C. Guivarch, K. Tachiiri, C.D. Jones, P. Ciais, Negative emissions physically needed to keep global warming below 2°C, Nat Commun. 6 (2015). https://doi.org/10.1038/ncomms8958.

[5] M. Lee, H. Lee, C. Seo, J. Lee, J.W. Lee, Enhanced energy efficiency and reduced CO2 emissions by hybrid heat integration in dimethyl carbonate production systems, Sep Purif Technol. 287 (2022). https://doi.org/10.1016/j.seppur.2022.120598.

[6] C. Seo, H. Lee, M. Lee, J.W. Lee, Energy efficient design through structural variations of complex heat-integrated azeotropic distillation of acetone-chloroform-water system, Journal of Industrial and Engineering Chemistry. 109 (2022) 306–319. https://doi.org/10.1016/j.jiec.2022.02.012.

[7] C. Seo, H. Lee, M. Lee, J.W. Lee, Temperature driven internal heat integration in an energy-efficient partial double annular column, Korean Journal of Chemical Engineering. 39 (2022) 263–274. https://doi.org/10.1007/s11814-021-0937-7.

[8] Y. Kim, H.S. Lim, M. Lee, M. Kim, D. Kang, J.W. Lee, Enhanced Morphological Preservation and Redox Activity in Al-Incorporated NiFe2O4for Chemical Looping Hydrogen Production, ACS Sustain Chem Eng. 9 (2021) 14800–14810. https://doi.org/10.1021/acssuschemeng.1c04619.

[9] Y. Kim, H.S. Kim, D. Kang, M. Kim, J.W. Lee, Enhanced redox performance of LaFeO3 perovskite through in-situ exsolution of iridium nanoparticles for chemical looping steam methane reforming, Chemical Engineering Journal. 468 (2023). https://doi.org/10.1016/j.cej.2023.143662.

[10] H.S. Kim, Y. Kim, H.S. Lim, H. Kim, J.W. Lee, Surface enrichment of lanthanum on Co3O4 for stable chemical looping combustion, Journal of CO2 Utilization. 73 (2023) 102532. https://doi.org/10.1016/j.jcou.2023.102532.

[11] J. Yang, D.W. Kang, H. Kim, B. Hwang, J.W. Lee, CO2-derived free-standing carbon interlayer embedded with molecular catalysts for improving redox performance in Li-S batteries, Chemical Engineering Journal. 451 (2023). https://doi.org/10.1016/j.cej.2022.138909.

[12] J. Yang, D.W. Kang, H. Kim, J.H. Park, W.Y. Choi, J.W. Lee, Fundamental role of Fe-N-C active sites in a CO2-derived ultra-porous carbon electrode for inhibiting shuttle phenomena in Li-S batteries, J Mater Chem A Mater. 9 (2021) 23660–23674. https://doi.org/10.1039/d1ta07415f.

[13] Y. Jang, E. Park, Social acceptance of nuclear power plants in Korea: The role of public perceptions following the Fukushima accident, Renewable and Sustainable Energy Reviews. 128 (2020). https://doi.org/10.1016/j.rser.2020.109894.

[14] X. Zhang, Y. Liu, Ultrafast removal of radioactive strontium ions from contaminated water by nanostructured layered sodium vanadosilicate with high adsorption capacity and selectivity, J Hazard Mater. 398 (2020). https://doi.org/10.1016/j.jhazmat.2020.122907.

[15] Y. Kim, Y.K. Kim, J.H. Kim, M.S. Yim, D. Harbottle, J.W. Lee, Synthesis of functionalized porous montmorillonite via solid-state NaOH treatment for efficient removal of cesium and strontium ions, Appl Surf Sci. 450 (2018) 404–412. https://doi.org/10.1016/j.apsusc.2018.04.181.

[16] A. Burger, I. Lichtscheidl, Stable and radioactive cesium: A review about distribution in the environment, uptake and translocation in plants, plant reactions and plants' potential for bioremediation, Science of the Total Environment. 618 (2018) 1459–1485. https://doi.org/10.1016/j.scitotenv.2017.09.298.

[17] A. Burger, I. Lichtscheidl, Strontium in the environment: Review about reactions of plants towards stable and radioactive strontium isotopes, Science of the Total Environment. 653 (2019) 1458–1512. https://doi.org/10.1016/j.scitotenv.2018.10.312.

[18] Y.K. Kim, S. Kim, Y. Kim, K. Bae, D. Harbottle, J.W. Lee, Facile one-pot synthesis of dual-cation incorporated titanosilicate and its deposition to membrane surfaces for simultaneous removal of Cs+ and Sr2+, Appl Surf Sci. 493 (2019) 165–176. https://doi.org/10.1016/j.apsusc.2019.07.008.

[19] H.H. Eom, Y. Kim, D. Harbottle, J.W. Lee, Immobilization of KTS-3 on an electrospun fiber membrane for efficient removal of Cs+ and Sr2+, J Environ Chem Eng. 9 (2021). https://doi.org/10.1016/j.jece.2021.105991.

[20] Y. Kim, H.H. Eom, D. Kim, D. Harbottle, J.W. Lee, Adsorptive removal of cesium by electrospun nanofibers embedded with potassium copper hexacyanoferrate, Sep Purif Technol. 255 (2021). https://doi.org/10.1016/j.seppur.2020.117745.

[21] J. Wang, S. Zhuang, Removal of cesium ions from aqueous solutions using various separation technologies, Rev Environ Sci Biotechnol. 18 (2019) 231–269. https://doi.org/10.1007/s11157-019-09499-9.

[22] H.K. Lee, B.M. Jun, S. Il Kim, J.S. Song, T.J. Kim, S. Park, S. Chang, Simultaneous removal of suspended fine soil particles, strontium and cesium from soil washing effluent using inorganic flocculants, Environ Technol Innov. 27 (2022). https://doi.org/10.1016/j.eti.2022.102467.

[23] R. Bengiat, B. Bogoslavsky, D. Mandler, J. Almog, Selective Binding and Precipitation of Cesium Ions from Aqueous Solutions: A Size-Driven Supramolecular Reaction, Chemistry - A European Journal. 24 (2018) 3161–3164. https://doi.org/10.1002/chem.201706181.

[24] F. Cai, F. Ma, X. Zhang, P. Reimus, L. Qi, Y. Wang, D. Lu, H.V. Thanh, Z. Dai, Investigating the influence of bentonite colloids on strontium sorption in granite under various hydrogeochemical conditions, Science of the Total Environment. 900 (2023). https://doi.org/10.1016/j.scitotenv.2023.165819.

[25] Y. Kim, H.H. Eom, Y.K. Kim, D. Harbottle, J.W. Lee, Effective removal of cesium from wastewater via adsorptive filtration with potassium copper hexacyanoferrate-immobilized and polyethyleneimine-grafted graphene oxide, Chemosphere. 250 (2020). https://doi.org/10.1016/j.chemosphere.2020.126262.

[26] Y.H. Cai, X.J. Yang, A.I. Schäfer, Removal of naturally occurring strontium by nanofiltration/reverse osmosis from groundwater, Membranes (Basel). 10 (2020) 1–23. https://doi.org/10.3390/membranes10110321.

[27] Z. Ye, Y. Zhang, L. an Hou, M. Zhang, Y. Zhu, Y. Yang, Preparation of a GO/PB-modified nanofiltration membrane for removal of radioactive cesium and strontium from water, Chemical Engineering Journal. 446 (2022). https://doi.org/10.1016/j.cej.2022.137143.

[28] H. Kim, H.H. Eom, Y. Kim, D. Harbottle, J.W. Lee, Reversible electro-mediated cesium ion removal using a zeolitic imidazolate framework derived zinc hexacyanoferrate composite, Chemical Engineering Journal. 450 (2022). https://doi.org/10.1016/j.cej.2022.138029.

[29] S. Khandaker, T. Kuba, S. Kamida, Y. Uchikawa, Adsorption of cesium from aqueous solution by raw and concentrated nitric acid-modified bamboo charcoal, J Environ Chem Eng. 5 (2017) 1456–1464. https://doi.org/10.1016/j.jece.2017.02.014.

[30] H.M. Yang, S.W. Kim, H.J. Kim, G.E. Lee, J.Y. Jang, Surface decontamination of radioactive cesium by a reversibly cross-linkable hydrogel using poly(vinyl alcohol) and phenylboronic acid-grafted poly(methyl vinyl ether-alt-mono-sodium maleate), Chemosphere. 339 (2023). https://doi.org/10.1016/j.chemosphere.2023.139617.

[31] B.K. Mahantesha, V. Ravindrachary, R. Padmakumari, R. Sahanakumari, P. Tegginamata, G. Sanjeev, V.C. Petwal, V.P. Verma, Effect of electron irradiation on optical, thermal and electrical properties of polymer electrolyte, J Radioanal Nucl Chem. 322 (2019) 19–27. https://doi.org/10.1007/s10967-019-06462-4.

[32] Y.K. Kim, K. Bae, Y. Kim, D. Harbottle, J.W. Lee, Immobilization of potassium copper hexacyanoferrate in doubly crosslinked magnetic polymer bead for highly effective Cs+ removal and facile recovery, Journal of Industrial and Engineering Chemistry. 68 (2018) 48–56. https://doi.org/10.1016/j.jiec.2018.07.028.

[33] H. Liu, A. Yonezawa, K. Kumagai, M. Sano, T. Miyake, Cs and Sr removal over highly effective adsorbents ETS-1 and ETS-2, J Mater Chem A Mater. 3 (2015) 1562–1568. https://doi.org/10.1039/C4TA06170E.

[34] C.C. Pavel, M. Walter, P. Pöml, D. Bouëxière, K. Popa, Contrasting immobilization behavior of Cs+ and Sr2+ cations in a titanosilicate matrix, J Mater Chem. 21 (2011) 3831–3837. https://doi.org/10.1039/c0jm03135f.

[35] A. Clearfield, D.G. Medvedev, S. Kerlegon, T. Bosser, J.D. Burns, M. Jackson, Rates of Exchange of Cs + and Sr 2+ for Poorly Crystalline Sodium Titanium Silicate (CST) in Nuclear Waste Systems, Solvent Extraction and Ion Exchange. 30 (2012) 229–243. https://doi.org/10.1080/07366299.2011.639256.

[36] L. Al-Attar, A. Dyer, A. Paajanen, R. Harjula, Purification of nuclear wastes by novel inorganic ion exchangers, J Mater Chem. 13 (2003) 2969. https://doi.org/10.1039/b308060a.

[37] J.G. Decaillon, Y. Andrès, B.M. Mokili, J.Ch. Abbé, M. Tournoux, J. Patarin, STUDY OF THE ION EXCHANGE SELECTIVITY OF LAYERED TITANOSILICATE $Na_3(Na,H)Ti_2O_2[Si_2O_6]_2 \bullet 2H_2O$, AM-4, FOR STRONTIUM, Solvent Extraction and Ion Exchange. 20 (2002) 273–291. https://doi.org/10.1081/SEI-120003027.

[38] F. Dixit, R. Dutta, B. Barbeau, P. Berube, M. Mohseni, PFAS removal by ion exchange resins: A review, Chemosphere. 272 (2021). https://doi.org/10.1016/j.chemosphere.2021.129777.

[39] Y.K. Kim, Y. Kim, S. Kim, D. Harbottle, J.W. Lee, Solvent-assisted synthesis of potassium copper hexacyanoferrate embedded 3D-interconnected porous hydrogel for highly selective and rapid cesium ion removal, J Environ Chem Eng. 5 (2017) 975–986. https://doi.org/10.1016/j.jece.2017.01.026.

[40] V.Q. Do, E.R. Reale, I.C. Loud, P.G. Rozzi, H. Tan, D.A. Willis, K.C. Smith, Embedded, micro-interdigitated flow fields in high areal-loading intercalation electrodes towards seawater desalination and beyond, Energy Environ Sci. (2023). https://doi.org/10.1039/d3ee01302b.

[41] W. Shi, J. Ma, F. Gao, R. Dai, X. Su, Z. Wang, Metal-Organic Framework with a Redox-Active Bridge Enables Electrochemically Highly Selective Removal of Arsenic from Water, Environ Sci Technol. 57 (2023) 6342–6352. https://doi.org/10.1021/acs.est.2c09683.

[42] R. Alam, M. Faheem, Y. He, X. Su, L. Zou, Ion selective electrosorption by two pseudocapacitive intercalating nanocomposite electrodes, Desalination. 566 (2023) 116923. https://doi.org/10.1016/j.desal.2023.116923.

[43] Y. Kim, K. Kim, H.H. Eom, X. Su, J.W. Lee, Electrochemically-assisted removal of cadmium ions by redox active Cu-based metal-organic framework, Chemical Engineering Journal. 421 (2021). https://doi.org/10.1016/j.cej.2021.129765.

[44] Y. Kim, H. Kim, K. Kim, H.H. Eom, X. Su, J.W. Lee, Electrosorption of cadmium ions in aqueous

solutions using a copper-gallate metal-organic framework, Chemosphere. 286 (2022). https://doi.org/10.1016/j.chemosphere.2021.131853.

[45] J.F. Gabitto, C. Tsouris, A review of transport models in charged porous electrodes, Frontiers in Chemical Engineering. 4 (2022). https://doi.org/10.3389/fceng.2022.1051594.

[46] R. Manikandan, C.J. Raj, M. Rajesh, B.C. Kim, J.Y. Sim, K.H. Yu, Electrochemical Behaviour of Lithium, Sodium and Potassium Ion Electrolytes in a Na0.33V2O5 Symmetric Pseudocapacitor with High Performance and High Cyclic Stability, ChemElectroChem. 5 (2018) 101–111. https://doi.org/10.1002/celc.201700923.

[47] S. Bodoardo, F. Geobaldo, N. Penazzi, M. Arrabito, F. Rivetti, G. Spanò, C. Lamberti, A. Zecchina, Voltammetric characterization of structural titanium species in zeotypes, Electrochem Commun. 2 (2000) 349–352. https://doi.org/10.1016/S1388-2481(00)00021-7.

[48] C. Yao, Y. Dai, S. Chang, H. Zhang, Removal of cesium and strontium for radioactive wastewater by Prussian blue nanorods, Environmental Science and Pollution Research. 30 (2022) 36807–36823. https://doi.org/10.1007/s11356-022-24618-w.

[49] E.A. Behrens, A. Clearfield, Titanium silicates, M3HTi4O4(SiO4)3·4H2O (M=Na+, K+),with three-dimensional tunnel structures for the selective removal of strontium and cesium from wastewater solutions, Microporous Materials. 11 (1997) 65–75. https://doi.org/10.1016/S0927-6513(97)00022-9.

[50] X. Liu, J. Wang, Adsorptive removal of Sr2+ and Cs+ from aqueous solution by capacitive deionization, Environmental Science and Pollution Research. 28 (2021) 3182–3195. https://doi.org/10.1007/s11356-020-10691-6.

[51] S.-H. Lee, M. Choi, J.-K. Moon, S.-W. Kim, S. Lee, I. Ryu, J. Choi, S. Kim, Electrosorption removal of cesium ions with a copper hexacyanoferrate electrode in a capacitive deionization (CDI) system, Colloids Surf A Physicochem Eng Asp. 647 (2022) 129175. https://doi.org/10.1016/j.colsurfa.2022.129175.

[52] K. Tang, Y. ha Kim, J. Chang, R.T. Mayes, J. Gabitto, S. Yiacoumi, C. Tsouris, Seawater desalination by over-potential membrane capacitive deionization: Opportunities and hurdles, Chemical Engineering Journal. 357 (2019) 103–111. https://doi.org/10.1016/j.cej.2018.09.121.

[53] P. Sylvester, T. Milner, J. Jensen, Radioactive liquid waste treatment at Fukushima Daiichi, Journal of Chemical Technology and Biotechnology. 88 (2013) 1592–1596. https://doi.org/10.1002/jctb.4141.

[54] A. Dyer, M. Pillinger, S. Amin, Ion exchange of caesium and strontium on a titanosilicate analogue of the mineral pharmacosiderite, J Mater Chem. 9 (1999) 2481–2487. https://doi.org/10.1039/a905549e.

[55] J. Sun, Q. Mu, T. Wang, J. Qi, C. Hu, Selective electrosorption of Ca2+ by MXene cathodes coupled with NiAl-LMO anodes through ion intercalation, J Colloid Interface Sci. 590 (2021) 539–547. https://doi.org/10.1016/j.jcis.2021.01.058.